SUBMITTED VERSION

This is the pre-peer reviewed version of the following article:

Mohammad Z. Rahman, Patrick C. Tapping, Tak W. Kee, Ronald Smernik, Nigel Spooner, Jillian Moffatt, Youhong Tang, Kenneth Davey, and Shi-Zhang Qiao
A benchmark quantum yield for water photoreduction on amorphous carbon nitride
Advanced Functional Materials, 2017; 27(39):1702384-1-1702384-11

which has been published in final form at http://dx.doi.org/10.1002/adfm.201702384
This article may be used for non-commercial purposes in accordance with Wiley Terms and Conditions for Use of Self-Archived Versions."

http://hdl.handle.net/2440/109268

A Benchmark Quantum Yield for Water Photoreduction on Amorphous Carbon Nitride

Mohammad Rahman, Patrick Tapping, Tak Kee, Ronald Smernik, Nigel Spooner, Jillian Moffatt, Youhong Tang, Kenneth Davey and Shi-Zhang Qiao*

M. Z. Rahman, Dr. Kenneth Davey, and Prof. S. Z. Qiao
School of Chemical Engineering, The University of Adelaide, SA 5005, Australia
E-mail: s.qiao@adelaide.edu.au

Dr. P. C. Tapping, Prof. T. W. Kee,
School of Physical Science, The University of Adelaide, SA 5005, Australia

Dr. R. Smernik
School of Agriculture, Food and Wine, The University of Adelaide, SA 5064, Australia

Prof. Nigel Spooner, Jillian Moffatt
Institute for Photonics and Advanced Sensing, The University of Adelaide, SA 5005, Australia

Dr. Youhong Tang
School of Computer Science, Engineering and Mathematics, Flinders University, SA 5001, Australia.

Abstract

Amorphous carbon nitride (a-CN) is a less-explored but a promising photocatalyst for hydrogen production. Despite its extended visible light absoprtion (EVLA), the extremely low quantum efficiency (QE) for water photoreduction to produce hydrogen is a long standing problem. This implies that EVLA is not proportionally translated into collection of large-amount photogenerated electrons. Minimizing the mismatch between light-absorption and charge-collection remains a great scientific challenge. Here we report a sponge-like hierarchical structure of a-CN that addresses this apparent mismatch. Combined experimental and finite difference time domain (FDTD) simulations demonstrate the ability of the a-CN sponge to induce scattering for total internal light reflection that promotes localized charge carrier generation. Diffused reflectance and transient fluorescence decay studies show good agreement with simulations with a 40 % enhanced light-trapping and an ~ 23 times longer

1

electron lifetime in spongy a-CN compared with that of the bulk material. The result is a new high benchmark for hydrogen production of 203.5 µmol h^{-1} with a QE of 6.1 % at 420 nm in a reaction system of 10 vol. % triethanolamine and 1 wt. % Pt cocatalyst. The enhanced water photoreduction is a result of amenable photophysical and electrochemical attributes existing within the a-CN sponge.

Keywords: Photocatalysis, carbon nitride sponge, water photoreduction, hydrogen production

1. Introduction

Crystalline carbon nitride (c-CN) and amorphous carbon nitride (a-CN) as a semiconductor have shown distinguished electro-optical and physicochemical properties and have become alternatives to metal-based semiconductors for photocatalytic hydrogen production via water-splitting.[1-6] c-CN is widely known as graphitic carbon nitride (GCN), and has been studied extensively (as is evident by hundreds of publications),[7] whilst research on a-CN as a photocatalyst remains relatively less (< 5 publications).[3-5] An advantage of a-CN over c-CN is its inherent ability of EVLA. However, the photocatalytic performance of a-CN is no way comparable to c-CN. For a-CN to compete with c-CN and metal-based systems, there is a real need to enhance the quantum yield in hydrogen production.

The reasons bulk a-CN shows low quantum yield in hydrogen production include: inefficient light-trapping, maximum photon-loss, short carrier lifetime, and; high-resistive charge transport. These factors are interdependent and establish a chain-effect for hydrogen production. In photocatalysis, hydrogen is produced through reduction of protons via water splitting,[8, 9]. Electrons are the initiator of the reduction reaction. The generation of electrons is possible only by absorption of photons with energy greater than intrinsic bandgap of the photocatalyst. However, the photogenerated electrons must survive recombination with holes to be separated and migrate from the bulk to surface where the reduction reaction takes place. A long lifetime of the electron and a low-resistive pathway promotes separation and transport

of the electrons.[10] Therefore an improvement in optical and electronic properties is necessary to overcome these shortcomings with bulk a-CN.

The QE and hydrogen production are complementary. Improvement in QE therefore depends simultaneously on i) improvement in trapping visible-light photons, and ii) efficient transfer of photogenerated carriers to the photocatalyst surface for redox reactions.[11] The light-trapping and electron separation of a semiconductor is strongly correlated to its crystal morphology and structural features at the nanometer level.[12] A controlled nanostructure beneficially increases visible light absorption, provides additional reactive sites, leads space-confined transport of charge carriers, and; exposures abundant edges and planes for reactants.[5, 9, 13]

As these attributes are best achieved in a nanostructure, we were guided to survey the list of diversified and custom-made 3D / 2D / 1D / 0D nanostructures of c-CN. Nanospheres (3D), nanosheets and nanomesh (2D), nanorods and nanowires (1D), nanodots (0D) etc. are notable nanostructures of c-CN.[14-18] Of these, 2D nanosheets of c-CN can be turned out as efficient nanostructures as a photocatalyst. However, blue-shift in photon absorption, limited exposed edges of high surface area, aggregation and, restacking caused by van der Walls interactions, are serious shortcomings with c-CN nanosheets limiting its exploitation in hydrogen photosynthesis.[19] Other nanostructures of c-CN have two common disadvantages: i) limited number of lateral edges, and ii) large proportion of inaccessible basal planes to reactants. These are considered significant barriers for high photocatalytic performance. On this basis we did not attempt to synthesize nanostructures of c-CN but looked to develop a new architecture for a-CN.

A comprehensive solution of the above mentioned problems can be attained through developing a hierarchical structure.[20] Essentially, a 3D hierarchical nano-structure comprises irregular fashioned multiple parallel and perpendicular planes, and thereby, provides abundant lateral edges and ready access to the basal planes. Recent demonstration of urchin-like

Fe$_3$O$_4$@Bi$_2$S$_3$, CdS@ZnO and CdS@Al$_2$O$_3$ heteroarrays with significantly enhanced catalytic degradation and hydrogen evolution efficiencies, underscored the superiority and effectiveness of hierarchical structures over planar structures with its associated problems.[21]

Here we synthesize a sponge-like hierarchical nanostructure of a-CN and demonstrate its photocatalytic hydrogen production. Results (discussed below) confirm this new hierarchical porous a-CN-sponge improves light absorption by incorporating scattering effect. Because of its unique shape and structure with interconnected porous networks, it enhances adsorption of reactants, facilitates transport of guest species to the binding sites, and; prevents aggregation. The result is an unprecedented new benchmark in photocatalytic activity. To the best of our knowledge, a sponge-like nanostructure of a-CN is yet to report.

The hierarchical nanostructures were usually prepared following two-step hard template or one-step sacrificial-template dissolution methods.[22] These methods require high cost of templates and tedious synthetic procedures which limit their practical applications in large-scale fabrication of photocatalysts. In contrast, the proposed nano-sponge can be developed through a self-templating strategy using a melamine sponge and dicyandiamide monomer as raw materials. When dicyandiamide soaked melamine-sponge was heated in aerobic condition, their co-polymerization resulted in the mesoporous sponge-like a-CN (*see* **Scheme S1**) with improved electro-optical and chemical properties.[2, 17] The entire process is straightforward, scalable and easy-to-perform (see experimental section).

2. Results

2.1 Morphology, structure and chemical features

The amorphous materials are featured by short-range atomic order in contrast to long-range atomic order for crystalline materials. The phases transition of the material can be readily distinguished by examining X-ray assisted diffraction patterns.[23] X-ray diffraction (XRD) and selective area electron diffraction (SAED) patterns were acquired to identify the

amorphous phases. As expected, the width of characteristic peaks at *ca.* 13º and 27º in XRD patterns is relatively flat and broadened when compared with c-CN (**Figure 1 a, b**). The rings in SAED patterns are also highly diffused (**Figure 2 a**). These results confirm the amorphous structure of the a-CN sponge.

The sponge-structure is decorated with porous micro-channels (*See* **Figure S1 a**). The combination of open pores and the micro-channels embedded in an amorphous matrix is beneficial from a photocatalytic point of view so as to achieve good infiltration, favorable mass transfer and charge separation, and; therefore, led to improved photocatalytic performance.[24] At this point, morphology of the as-prepared a-CN sponge was studied using Transmission Electron Microscopy (TEM) and Scanning Electron Microscopy (SEM). SEM images show clearly the interlayered galleries of 3D sponge-like structures (**Figure 2 b, c**) in which interlayers are in both perpendicular and parallel directions to the basal planes. TEM images (**Figure 2d, e** and **Figure S2**) show that the layers are composed of interconnected nanosheets. The voids indicate a disjoint in nanosheets due to hollows giving rise to distributed hierarchical pores. This is beneficial for space-confined transport of charge carriers within the layers and spatial separation of redox active sites between the lateral edges and basal planes.[5, 25]

As is shown in SEM images, the individual layer comes with distributed micro-channels and decorated all over the perimeter of pores (*see* **Figure S1**). The Barret-Joyner-Halenda (BJH) pore-size distribution (**Figure 3 a**) showed that few micropores (< 2 nm) are intermingled among abundant mesopores (2-50 nm). These bimodal interconnected pores create effective channels (**Figure 3 b, c**) for the transport of reactant molecules to reactive sites on the pore walls. Consequently, reactant molecules can readily diffuse into the reaction sites and the products can also freely move out of them.[26] As a result, the enhanced adsorption and diffusion kinetics of reactants in the new porous a-CN sponge can significantly

reduce the mass-transport barriers and accelerate the chemical activation rates of adsorbed species.[27]

For photocatalysis it is necessary to keep π-conjugated system intact in the carbon nitride.[28] In the representing XRD patterns (**Figure 1 b**), a-CN sponge exhibits two typical peaks near 13º and 27º – this suggests preserving of the basic structure of π-conjugated system.[1, 3] This observation is in good agreement with the results of solid-state ^{13}C CP-NMR spectra (**Figure 4 a, b** and **Figure S3**) in which the peaks at ~157 ppm and ~165 ppm are evidence of heptazine tectons and poly(tri-*s*-triazine) structures that are usually found in carbon nitride solids.[29] As shown in Appendix A1, both the c-CN and a-CN hold the same ppm positions for different carbon nodes in NMR spectra, which are in line with that of bulk melem (an intermediate of carbon nitride).

The preservation of π-conjugated system was further substantiated by investigating the chemical states of a-CN sponge through Fourier transform infra-red (FTIR) and Raman spectral studies. The a-CN sponge resembles the peaks (from vending and stretching vibration of C-N heterocycles) of core carbon nitride in the representative FTIR and Raman spectra, substantiating preservation of π-conjugated system. For example, the pronounced peak at 809 cm^{-1} in FTIR spectra (**Figure S4**) and Raman peak near 700 cm^{-1} (**Figure S5**) indicate the retention of triazine units of melon which is the core structure of carbon nitride.[15] However, C-N heterocycles peaks are diffused due to the short-range order between C and N atomic arrangement in a-CN sponge.[4]

The Raman peaks between 800 to 1400, cm^{-1} and the FTIR peaks between 1200 to 1600, cm^{-1} are from the stretching vibrations of C-N heterocycles.[2] The strong signal in the range of 3300 to 3600, cm^{-1} of FTIR spectra is a result of high volume of adsorbed hydroxyl groups, or water molecules, indicating abundant active sites in the sponge-like a-CN.[15] The chemical structure and composition of a-CN sponge is further substantiated through deconvoluted X-ray Photoelectron Spectroscopy (XPS) data. In the deconvoluted C1s spectra

(**Figure 4 c**), together with two characteristic peaks (i.e. sp^2 C-C bond @ 284 eV and N-C=N bond of aromatic rings @ 288 eV), a third peak at 286 eV can be observed.[2, 15] This additional peak might appear as a consequence of extra nitrogen-loss during amorphization to a-CN. The hypothesis of nitrogen-loss is supported by the decreased C/N molar ratio from 0.68 for c-CN to 0.73 for a-CN sponge. This is consistent with previous results.[2, 30] The peaks in deconvoluted N1s spectra (**Figure 4 d**) are composed of sp^2 C=N-C at 397.5 eV, N(-C)$_3$ at 398.2 eV and C-N-H groups at 401 eV, respectively.[2, 15]

2.2 Light Scattering, trapping and absorption

EVLA is a key determinant for improving the photocatalytic performance (i.e. QE). Amorphization was reported to be effective in increasing visible light absorption. For example, Kang et al. showed that the intrinsic band-to-band absorption edge of a-CN (extrapolated from UV-Vis diffused reflectance spectra) was extended to ~ 690 nm, whilst the absorption edge of crystalline carbon nitride varied between 400 to 500, nm.[1, 14] The long-range atomic disorder was shown as a reason to entail long tail absorption.[4, 31] This redshift of absorption edge therefore ascribes imperious optical advantage of a-CN.

Comparable to previous results, the UV-Vis spectra of a-CN sponge shows a broad absorption spectrum with a strong tail in the range of 500 to 800, nm (**Figure 5**). However, the structural and morphological asymmetry of a-CN sponge renders distinct optical and electronic properties in comparison with reported bulk a-CN. We persuaded Yee's finite difference time domain (FDTD) approach to understand how light interacts with both planar and spongy a-CN.[32] FDTD is an established and widely accepted method to solve Maxwell's electromagnetic equations to explore the behavior of a propagating electromagnetic wave (i.e. light) through a material medium.[33] In FDTD approach, Maxwell's equations are replaced by a set of finite difference equations with defined boundary conditions.[32, 34]

7

As is shown in **Figure 6a**, our simulation results show that light propagates without any internal reflection in a planar structure of a-CN whereas, a significant portion of the propagating light gets internally reflected in the sponge-air interface before radiating into the vacuum. This confirms that the hierarchical architecture allows internal light-scattering. Moreover, the open pores act like as optical cavities that give rise to interference between forward and backward propagating light [35-37] that enhance the probability of light-matter interaction in subwavelength pores. As a result, hierarchical a-CN sponge provides an increased number of light travelling paths with enhanced interaction time and absorption efficiency inside the pores, and thereby impart controlled-light absorption.[38]

We further extended our investigation to understand the the impact of scattering induced multiple internal reflection inside the pores of a-CN sponge through diffused reflectance studies. This allowed us to quantify the external light reflection rate of both planar and a-CN sponge. As is shown in **Figure 6b**, the light reflectance reaches to 85% in planar a-CN, whereas this rate is less than 35 % in the case of hierarchical a-CN sponge, confirming a 40 % improvement in light absorption. These results are therefore in good agreement with the simulations.

The combined simulation and experimental results substantiate the significant improvement in light collection efficiency as a result of internal light reflection due to scattering induced by the interconnected mesoporous channels in a-CN sponge. Considering positive impacts of increased light harvesting, this hierarchical a-CN sponge is expected to be an efficient photocatalyst.

2.3   Charge separation and transport

The sponge-like morphology facilitates the efficient light-trapping through multiple internal reflections inside the porous hollow structure, thus abruptly reducing the light transmission.

Aside from greater photon absorption, an improvement in charge separation-transfer efficiency is essential for increasing the QE in hydrogen production.

Hydrogen production follows the reduction reaction of protons. Electrons are used for reduction of the protons. The transport of electrons from bulk of the material to the surface is an important matter of concern. The separation and transport of charge carriers is a quality of a material that is governed by conductivity, mobility and recombination activities of the charge carriers.[39] Carbon nitride is an n-type semiconductor. A positive slop in Mott-Schottky(M-S) plot is an indication of the n-type conductivity.[3] In n-type semiconductor, conductivity is mainly due to movement of electrons as majority carriers. Therefore, position of Fermi-level *w. r. t.* conduction band (CB) is rate determining for trapping/recombination, and electron transfer to CB (the electrons in CB is given emphasis because they are necessary for proton reduction to hydrogen). The quasi Fermi level was determined from M-S analysis, **Figure 7 a**. A quasi Fermi level that is adjacent to CB is beneficial for electron transfer. The data show that the quasi Fermi level of a-CN sponge is -0.5 V *vs.* RHE (reversible hydrogen electrode) at pH = 0, whilst the quasi Fermi level of carbon nitrides reported in the literature varied between -0.9 to -1.3, V vs RHE at pH = 0.[2, 3, 31, 40] This means that the quasi Fermi level of a-CN sponge is more down-shifted than traditional carbon nitrides. This downshift is correlated to lower flat-band potential that indicates greater electrical conductivity of a-CN sponge.[41] The greater electrical conductivity is, in turn, the result of greater mobility of charge carriers. This high-mobility assists faster separation of photogenerated electron-hole pairs and diminishes the possibility of electron-hole recombination/surface trapping at sub-bandgap energy levels.[41, 42] Because of its principle of operation, we acquired steady-state photoluminescence (PL) spectra to assess the extent of suppression of band-to-band recombination of electron-hole pairs. The significant reduction in photoluminescence intensity for a-CN sponge compared to the planar sample (**Figure 7 b**) highlights suppression of charge carrier recombination.[3, 17, 18]

9

Recombination is a process in which an excited electron falls back to ground state, combines with a hole, and; both electron and hole annihilate.[43] A suppression of recombination rate therefore is possible if: i) the electrons and holes are delocalized, and; ii) electrons have longer lifetime. In a-CN sponge the destruction of long-range atomic order and partial loss of nitrogen atoms result in an extended tail absorption which is related to localized states close to band edges.[5] These localized states create shallow trap-states to capture the electrons and delocalize them from holes in valence band. This suppresses recombination.[44] Moreover, the hierarchical pores provide a reduced diffusion length for electrons to travel from the bulk to lateral edges of pore walls within the layers, and therefore, culminate in active separation of photogenerated electron-hole pairs.[4, 17] We further investigated the reasons for suppression of recombination through time-resolved fluorescence spectroscopy. This gives information about the time averaged lifetime of electrons. The time resolved spectroscopy data (**Figure 7 c, d**) show that the effective lifetime of electrons in the case of bulk a-CN is a factor of ~23 times shorter than the spongy a-CN. This result confirms the reason for the suppressed recombination manifested by PL studies in a-CN sponge. The significantly shorter lifetime of electrons in bulk a-CN is the principal reason for its low quantum yield in hydrogen production.

We carried out electroimpedance measurements to corroborate the separation efficiency and kinetic barrier for electrons and holes. The results are shown in the form of Nyquist plot. As is shown in **Figure S6**, the Nyquist plots are composed of two semicircles bounded by respective low and high frequency regions. The origin of the two semicircles is related to the combined effect of the capacitance of depletion layer and photocatalyst/electrolyte double layer interfaces.[45] These capacitances are a function of frequency. In the low frequency region, double layer capacitance is controlling whilst, at high frequency, depletion layer capacitance is controlling.[41] The charges that transfer through hotocatalyst/electrolyte double layers initiate the redox reactions, and depletion layer created

10

due to charge transfer contributes to photocurrent generation.[46] In both cases, low charge transfer resistance is always favorable for greater rates of redox reactions and photocurrent.[47] A measure of the low resistance is the semicircles with shorter diameter in the Nyquist plot.[48] As is shown in **Figure S6**, semicircles in case of a-CN sponge have the shorter diameter than that of the bulk, meaning that the charge transfer resistance of depletion layer and double layer is highly reduced in a-CN sponge.

The enhancement in photon absorption and reduction in charge transfer resistance can boost the level of current for hydrogen production. Keeping this in mind, we have performed voltammetry and transient photocurrent measurements to substantiate the impact of low transfer resistance and high photon absorption capability of a-CN sponge. As is shown in **Figure S7**, the current density for a-CN sponge is greater than that of the bulk. A positive shift in onset potential (the potential at which photocurrent density is -1 mA cm^{-2}) can also be seen, suggesting that the kinetic barrier for hydrogen evolution is reduced in a-CN sponge. The transient photocurrent responses are presented in **Figure S8**. The photocurrent in a-CN sponge is much enhanced compared with the bulk, confirming that the charge separation has been improved.[2, 31] The porous micro-channels, aligned in a parallel-perpendicular layered fashion in a-CN sponge, are key reasons for stemming high performance in photocurrent and charge transport processes. This is because this particular arrangement of porous channels promotes electron delocalization on surface terminal sites and enhances transport along in-plane direction by shortening the charge carrier's diffusion length.[15] Moreover, the greater on/off ratio of photocurrent in a-CN sponge compared with the bulk strongly suggests a lack of electron-hole recombination due to surface trapped charge carriers.[41]

The impedance, voltammetry and photocurrent measurements strongly support the hypothesis that spongy a-CN has necessary electro-optical and physicochemical attributes for high hydrogen production.

11

3. Photocatalytic Performance

The photocatalytic activities of a-CN sponge were evaluated by detecting evolved hydrogen in an aqueous solution containing 10 vol. % triethanolamine as a hole scavenger and 1 wt. % Pt as a cocatalyst under visible light irradiation ($\lambda = 420$ nm). As is shown in **Figure 8a**, the a-CN sponge shows a new high bench-mark for hydrogen production of 203.5 μmol h^{-1} compared with the much lower 1.2 μmol h^{-1} for bulk a-CN (*see* **Table S1** for comparison with previous results). This lower rate of hydrogen production implies that light absorption is not proportionally translated to large-amount collection of electrons by bulk a-CN. With a ~170 times greater hydrogen production it reasonable to conclude that the apparent mismatch between light-absorption and charge collection is significantly compensated for in the spongy a-CN.

We executed three experimental runs of photocatalysis testing, each of 4 h of consecutive irradiation, and measured hydrogen production at each hour. There was a 15 day storage period of the reaction system between each run. Therefore the final run (3rd) was carried out on day 45. We did not observe significant deterioration in overall hydrogen production between 1st, 2nd and 3rd runs. This non-degradable cyclic hydrogen production (**Figure 8b**) showed that a-CN sponge is not only highly active but that it is therefore a robust photocatalyst too. In addition to photocatalytical stability, the comparative studies of XRD, FTIR and UV-Vis measurements of fresh samples and used samples (see **Figure S9**) showed negligible change in the respective spectra. This confirms the structural, chemical and optical stability of a-CN sponge and its re-usability as a photocatalyst.

The apparent quantum efficiency (AQE) is a measure of the degree of improvement in photocatalytic efficiency of a photocatalyst. In this regard, we performed measurements to determine the AQE of a-CN sponge under the same photocatalytic condition of hydrogen production at wavelengths of 420, 475, 550, and 600, nm. The calculated AQE of a-CN sponge is 6.1, 1.4 and 0.2 % at 420, 475 and 550, nm, respectively (**Figure 8 c**). There was no

hydrogen production observed at 600 nm. An AQE of 6.1 % at 420 nm was the greatest for a-CN as a photocatalyst. This new bench-mark value of AQE is, by definition, strong evidence of maximization of photon gain - indicating that a great number of absorbed incident photons took part in photogeneration of electron-hole pairs, and that the electrons reached the catalyst surface to initiate proton reduction. This finding highlights that a morphological fine-tuning is effective in enhancing AQE of the a-CN photocatalyst.

The a-CN sponge showed a broad visible light absorption spectra which was extended to 800 nm. It is therefore reasonable to assume that a-CN sponge would have had an AQE of much greater value than 6.1 %. However, the computed AQE indicates that a-CN sponge is not active in hydrogen production > 550 nm - despite a long tail absorption of 550 to 800, nm. This contrasts significantly with previous results of maximum wavelength for hydrogen production of over 600 nm.[4] It is actually possible that there was hydrogen production at 600 nm, but that it was minute such that it could not be detected in the gas chromatograph. Aside from this limitation, the main reason behind the discrepancies might be the lower probability of excitation of valence electrons to the conduction band under the longer wavelength irradiation[3, 49]. We investigated this by computing the electronic bandgap using Kubelka-Munk (K-M) technique. The K-M plot of a-CN sponge showed that there is an intrinsic bandgap of 2.16 eV and a band tail of ~ 1 eV (see **Figure S10**). This intrinsic bandgap is related to an absorption edge of ~ 574 nm which is fall within limit of maximum wavelength of 550 nm for active hydrogen production. By contrast, the band tail is lower than the minimum potential (1.23 eV in ideal case, 2.0 eV if an over potential is taken into account) necessary for water-splitting. This is of no use from a thermodynamics standpoint. It should therefore be clear why in fact that there is no hydrogen production beyond the intrinsic absorption edge. This problem might be resolved by creating mid-gap energy states to accommodate the electrons excited by lower energy photons. A useful way to create mid-gap

13

states is doping heteroatom.[31] Another possibility is incorporating Anderson-localized photon modes.[37] This is beyond the scope of the present work however.

4. Discussion

Interest is shown in a-CN as a photocatalyst because of its inherent tendency to show EVLA – a key requirement for efficient hydrogen production. On the basis of findings reported here, the lower hydrogen evolution with bulk a-CN indicates that it is unable to make the best use of its EVLA ability due to inefficient charge collection. Arguably this means that bulk a-CN might maximize wasted absorption in the region where the electron-hole pairs are lost to recombination.[35]

The key findings for improved hydrogen production in a-CN sponge can be summarized as follows: Amorphization led to a modified atomic arrangement with adsorption edges in longer wavelength; The hierarchical structure of spongy a-CN induced light scattering and facilitated light-trapping inside the pore as well as in the interior of cavities to increase photon absorption in extended visible light with abundant charge carrier generation; The mesoporous structure of nano-sponge delocalizes the photogenerated electrons and enhances the charge migration along in plane direction by reducing the diffusion length - and increases the charge carrier mobility and electrical conductivity; Charge carrier delocalization effectively suppresses the band-to-band recombination and augments the charge separation efficiency; Low charge transfer resistance ensures efficient transfer of charge carriers to the surface where redox reactions take place, and; The low onset potential, a manifestation of reduced kinetic barrier, was highly favorable for a new high benchmark for hydrogen production in the a-CN sponge.

The significant increase in quantum yield compared with bulk a-CN underscores the excellent electro-optical and physicochemical properties of a-CN sponge as a photocatalyst. Despite a lack of a meaningful contribution from tail absorption, a QE of 6.1% resulted due to

abundant charge carrier generation by photons of intrinsic absorption wavelength and efficient collection of electrons for reduction reactions. Research now needs to be carried out to make use of tail absorption in water photoreduction. An increase in QE might be possible by creating mid-gap states and practicing Anderson-localized photon modes.

5.   Conclusions

Hierarchical sponge-like a-CN has been reported for the first time as a hydrogen evolution photocatalyst. It addresses an apparent mismatch between optical absorption and charge collection in bulk a-CN. The new morphology has optimized structural, electro-chemical and optical properties. It can be synthesized using easily available and cheap raw materials. A new high benchmark hydrogen production was achieved of 203.5 μmol h^{-1} with an apparent quantum efficiency of 6.1% at λ = 420 nm. Due to its extended visible light absorption edge and excellent charge separation and transport ability, sponge-like a-CN appears a promising material for optoelectronics and photovoltaic applications. Because of its lower barrier potential it may promote the faradic reaction rate and should therefore be exploitable for electrocatalysis and applications in fuel cells. Additional carbon-based photocatalysts could be synthesized combining both metal and metal-free elements.

6.   Experimental Section

Synthesis of a-CN sponge: The melamine-sponge was cut into thin pieces (*ca.* 0.2 cm thick). A saturated solution of dicyandiamide was prepared by adding 15 g of dicyandiamide into 60 mL of mili-Q water. The solution was stirred and sonicated at room temperature (RT) for 30 mins to obtain a homogeneous white-suspension. The as-cut pieces of melamine-sponge were then soaked in the dicyandiamide suspension and kept there for 2 h at RT. After drying overnight in a vacuum oven, dicyandiamide soaked sponge then was placed in a ceramic boat to heat in a long-tube furnace (600 ℃ @ 2 ℃ min^{-1}, 4 h) under nitrogen flow. Following cooling of the furnace, the agglomerate was collected and grinded into powder for

15

characterizations. The bulk c-CN and a-CN were prepared from dicyandiamide and thiourea, respectively, following procedures described elsewhere.[1, 4]

Characterization: Spectroscopy images of a-CN sponge were obtained by SEM (Quanta 450) and TEM (Tecnai G2 spirit) instruments. The XRD pattern was recorded using X-ray diffractometer (Miniflex, Rigaku) at 40 kV and 15 mA with Cu Kα radiation (λ = 0.154178 nm). Solid state ^{13}C NMR spectra were obtained from a Bruker 200 AVANCE spectrometer equipped with a 4.7 T wide-bore superconducting magnet operating at a ^{13}C resonant frequency of 50.33 MHz. A FTIR spectrometer (Nicolet 6700) was used to obtain Fourier transform infra-red spectra. Raman spectra were collected by iHR550 Raman microscope (HORIBA scientific). An AXIS ultra-spectrometer (Kratos Analytical Ltd., GB) was used to obtain XPS spectra. UV-Vis spectrophotometer (UV2600, Shimadzu, Japan) was used to analyze optical diffuse reflectance spectra (DRS). Photoluminescence (PL) spectra were measured at RT using a fluorescence spectrometer (RF-5301PC, Shimadzu, Japan). N_2 adsorption-desorption measurements were carried out in a BELSORP-max instrument (BELJapan Inc.) Time resolved measurements for a-CN sponge were conducted using an Edinburgh Instruments F980 spectrofluorimeter, with an Opotek OPO 5 ns pulse width 20 Hz laser tuned to 410 nm for illumination and a Hamamatsu air-cooled R928 photomultiplier for detection. The sample was in powder-form, and was placed in a UV to NIR-transparent fused quartz cuvette for measurements. The monochromator was set to detect emissions at 515 nm and the PMT output was read directly via an oscilloscope. Single pulses were detected and measured to prevent pulse-jitter broadening the output. Fluorescence lifetime data for bulk a-CN were obtained using a fluorescence upconversion spectrometer in transmission mode (Ultrafast Systems, Halcyone). A Ti:sapphire regenerative amplifier (Spectra-Physics, Spitfire Pro XP 100F) was used as the source of excitation and gate beams, producing pulses with a duration of 100 fs at a 1 kHz repetition rate. The excitation wavelength of 400 nm was generated by frequency doubling the 800 nm fundamental using a 0.5 mm BBO crystal.

Photocatalytic H₂ and AQE measurements: In a three-necks Pyrex flask, 100 mg of photocatalyst was dispersed in a solution containing 80 mL of 10 vol. % triethanolamine and 1 wt. % H_2PtCl_6 was added as a source of Pt. The openings of the flask were sealed with silicone rubber septa. The mixture was degassed by argon flow for 30 min. Following degassing, the reactor was irradiated by a light source (300 W Xenon arc lamp) mounted with a 420 nm cut-off filter. The evolved gas was sampled through an on-line gas chromatograph (Clarus 480, Perkin-Elmer) every hour and the rate of hydrogen production was quantified. The gas chromatograph (GC) consisted of 5 Å molecular sieve column and a built-in thermal conductivity detector. For GC, Ar was used as a carrier gas. The experiment was carried out at RT and atmospheric pressure.

Quantum efficiency was computed following the method described by Liu et al.[50] The catalyst solution was irradiated for 1 h by a 300 W Xe arc lamp using a 420, 475 and 550, nm band-pass filters. The average intensity of irradiation was determined to be 17, 14.7 and 10.2, mW cm^{-2}, respectively, by a spectroradiometer; the irradiation area was ~ 3 cm^2. AQE was computed using following equation:[3]

$$AQE = \frac{2 \times number\ of\ evolved\ hydrogen\ molecules}{Number\ of\ incident\ photons} \times 100\% \qquad (1)$$

Photo-electrochemical measurements: Using doctor-blade method, a working electrode was prepared by coating slurry on fluorine-doped tin-oxide (FTO) glass electrode (2 x 1.5, cm) and drying in an oven under nitrogen flow (350 °C for 30 min). The slurry was made by grinding 0.1 g of photocatalyst with 0.03 g of polyethylene glycol (PEG) in 0.5 mL of ethanol. The measured film thickness of the electrode was around 10 to 11, μm. The Mott-Schottky measurement was performed using an *impedance-potential* methods where the frequency was set to 1 kHz over the potential range -0.4 V to +0.4 V, and 0.2 M Na_2SO_4 was used as electrolyte. For transient photocurrent measurement, a 300 W Xenon arc lamp light was chosen as a light source while 0.2M Na_2S + 0.05 M Na_2SO_3 aqueous solution was as

electrolyte at 0.5 V bias. The Electro-Impedance Spectroscopy (EIS) measurements were recorded over a 0.005 to 10^5 Hz frequency range with ac amplitude of 10 mV and 0.5 M Na_2SO_4 was used as electrolyte. Linear-sweep voltammetry curves were obtained in a sweep range of -0.3 to -2.0, V with a scan rate of 5 mV s^{-1}. All experiments were carried out in a three-electrode system electrochemical analyzer (CHI 650D instruments). The prepared sample was used as the working electrode with an active area of about 1.35 cm^2, a Pt wire as the counter electrode, and; Ag/AgCl (saturated KCL) as the reference electrode.

FDTD simulation: The simulation was performed in an interactive FDTD toolbox that works within MATLAB. The toolbox comes with an embedded graphical user interface (GUI) in which all simulation parameters can be defined. Perfectly matched layer (PML) boundary conditions were included for geometrical structures.

Supporting Information

Supporting Information is available from the Wiley Online Library or from the author.

Received: ((will be filled in by the editorial staff))
Revised: ((will be filled in by the editorial staff))
Published online: ((will be filled in by the editorial staff))

[1]   X. Wang, K. Maeda, A. Thomas, K. Takanabe, G. Xin, J. M. Carlsson, K. Domen, M. Antonietti, *Nat. Mater.* **2009**, *8*, 76.

[2]   M. Z. Rahman, J. Ran, Y. Tang, M. Jaroniec, S. Z. Qiao, *J. Mater. Chem. A* **2016**, *4*, 2445.

[3]   M. Z. Rahman, J. Zhang, Y. Tang, K. Davey, S.-Z. Qiao, *Mater. Chem. Front.* **2017**, *1*, 562.

[4]   Y. Kang, Y. Yang, L.-C. Yin, X. Kang, G. Liu, H.-M. Cheng, *Adv. Mater.* **2015**, *27*, 4572.

[5]   Y. Kang, Y. Yang, L. C. Yin, X. Kang, L. Wang, G. Liu, H. M. Cheng, *Adv. Mater.* **2016**, *28*, 6471.

[6]   Y. Xu, M. Kraft, R. Xu, *Chem. Soc. Rev.*, **2016**, *45*, 3039.

[7]   W. J. Ong, L. L. Tan, Y. H. Ng, S. T. Yong, S. P. Chai, Chem Rev 2016; J. Wen, J. Xie, X. Chen, X. Li, *Appl. Surface Sci.* **2017**, *391*, 72.

[8]   D. Ravelli, D. Dondi, M. Fagnoni, A. Albini, Chemical Society Reviews 2009, 38, 1999; S. Fukuzumi, Y. Yamada, T. Suenobu, K. Ohkubo, H. Kotani, *Energy Environ. Sci.* **2011**, *4*, 2754.

[9]   M. Z. Rahman, C. W. Kwong, K. Davey, S. Z. Qiao, *Energy Environ. Sci.* **2016**, *9*, 709.

[10]   A. S. Rury, T. E. Wiley, R. J. Sension, *Acc. Chem. Res.* **2015**, *48*, 860.

[11]   N. Serpone, A. V. Emeline, V. K. Ryabchuk, V. N. Kuznetsov, Y. M. Artem'ev, S. Horikoshi, *ACS Energy Lett.* **2016**, *1*, 931.

[12]   a) R. S. Sprick, B. Bonillo, R. Clowes, P. Guiglion, N. J. Brownbill, B. J. Slater, F. Blanc, M. A. Zwijnenburg, D. J. Adams, A. I. Cooper, *Angew. Chem. Int. Ed.* **2016**, *55*, 1792; b) A. G. Slater, A. I. Cooper, *Science* **2015**, *348*, 988.

[13]   S. C. Warren, K. Voïtchovsky, H. Dotan, C. M. Leroy, M. Cornuz, F. Stellacci, C. Hébert, A. Rothschild, M. Grätzel, *Nat. Mater.* **2013**, *12*, 842.

[14]   S. Yang, Y. Gong, J. Zhang, L. Zhan, L. Ma, Z. Fang, R. Vajtai, X. Wang, P. M. Ajayan, *Adv. Mater.* **2013**, *25*, 2452.

[15]   J. Zhang, M. Zhang, C. Yang, X. Wang, *Adv. Mater.* **2014**, *26*, 4121.

[16]   Q. Han, B. Wang, J. Gao, Z. Cheng, Y. Zhao, Z. Zhang, L. Qu, *ACS Nano* **2016**, *10*, 2745.

[17]   Q. Liang, Z. Li, X. Yu, Z. H. Huang, F. Kang, Q. H. Yang, *Adv. Mater.* **2015**, *27*, 4634.

[18]   Q. Liang, Z. Li, Z.-H. Huang, F. Kang, Q.-H. Yang, *Adv. Funct. Mater.* **2015**, *25*, 6885.

[19]   J. Zhang, Y. Chen, X. Wang, *Energy Environ. Sci*. **2015**, *8*, 3092.

[20]   a) W. J. Roth, B. Gil, W. Makowski, B. Marszalek, P. Eliasova, *Chem. Soc. Rev.*, **2016**, *45*, 3400; b) M. H. Sun, S. Z. Huang, L. H. Chen, Y. Li, X. Y. Yang, Z. Y. Yuan, B. L. Su, *Chem. Soc. Rev.* **2016**, *45*, 3479.

[21]   a) S. Luo, F. Chai, L. Zhang, C. Wang, L. Li, X. Liu, Z. Su, *J. Mater. Chem.* **2012**, *22*, 4832; b) D. Barpuzary, Z. Khan, N. Vinothkumar, M. De, M. Qureshi, *J. Phys. Chem. C* **2012**, *116*, 150.

[22]   X. Li, J. Yu, M. Jaroniec, *Chem. Soc. Rev*. **2016**, *45*, 2603.

[23]   A. K. Cheetham, A. L. Goodwin, *Nat. Mater.* **2014**, *13*, 760.

[24]   W. Kim, E. Edri, H. Frei, *Acc. Chem. Res.* **2016**, *49*, 1634.

[25]   a) M. Cargnello, B. T. Diroll, *Nanoscale* **2014**, 6, 97; b) D. Schneider, D. Mehlhorn, P. Zeigermann, J. Karger, R. Valiullin, *Chem. Soc. Rev.,* **2016***, 45,3439.*

[26]   W. Ho, J. C. Yu, S. Lee, *Chem. Commun.*, **2006**, 1115.

[27]   Z. Y. Yuan, T. Z. Ren, B. L. Su, *Adv. Mater.* **2003**, *15*, 1462.

[28]   M. Zhang, X. Wang, *Energy Environ. Sci.* **2014**, 7, 1902.

[29]   a) J. Sun, J. Zhang, M. Zhang, M. Antonietti, X. Fu, X. Wang, *Nat. Commun.* **2012**, *3*, 1139; b) A. Schwarzer, T. Saplinova, E. Kroke, *Coord. Chem. Rev.* **2013**, *257*, 2032.

[30]   P. Niu, G. Liu, H.-M. Cheng, *J. Phys. Chem. C* **2012**, *116*, 11013.

[31]   J. Ran, T. Y. Ma, G. Gao, X.-W. Du, S. Z. Qiao, *Energy Environ. Sci*. **2015**, *8*, 3708.

[32]   Y. Kane, *IEEE Trans. Antennas Propag.* **1966**, *14*, 302.

[33]   M. Morgan, D. Fisher, E. Milne, *IEEE Trans. Antennas Propag.* **1987**, *35*, 191.

[34]   W. P. Huang, C. L. Xu, W. Lui, K. Yokoyama, *IEEE Photon. Technol. Lett.* **1996**, *8*, 649.

[35]   H. Dotan, O. Kfir, E. Sharlin, O. Blank, M. Gross, I. Dumchin, G. Ankonina, A. Rothschild, *Nat. Mater.* **2013**, *12*, 158.

[36]   M. L. Brongersma, Y. Cui, S. Fan, *Nat. Mater.* **2014**, *13*, 451.

[37]   M. Aeschlimann, T. Brixner, D. Differt, U. Heinzmann, M. Hensen, C. Kramer, F. Lükermann, P. Melchior, W. Pfeiffer, M. Piecuch, C. Schneider, H. Stiebig, C. Strüber, P. Thielen, *Nat. Photon.* **2015**, *9*, 663.

[38]   a) H. Li, Z. Bian, J. Zhu, D. Zhang, G. Li, Y. Huo, H. Li, Y. Lu, *J. Am. Chem. Soc.* **2007**, *129*, 8406; b) J. Yu, H. Yu, H. Guo, M. Li, S. Mann, *Small* **2008**, *4*, 87.

[39]   a) M. J. Muñoz-Batista, A. Kubacka, A. B. Hungría, M. Fernández-García, *J. Catal.* **2015**, *330*, 154; b) L. Hammarstrom, *Acc. Chem. Res.* **2015**, *48*, 840.

[40]   Y. Li, R. Jin, Y. Xing, J. Li, S. Song, X. Liu, M. Li, R. Jin, *Adv. Energy Mater.* **2016**, 6, 1601273.

[41]   U. Sim, J. Moon, J. An, J. H. Kang, S. E. Jerng, J. Moon, S.-P. Cho, B. H. Hong, K. T. Nam, *Energy Environ. Sci.* **2015**, *8*, 1329.

[42]   a) U. Sim, T.-Y. Yang, J. Moon, J. An, J. Hwang, J.-H. Seo, J. Lee, K. Y. Kim, J. Lee, S. Han, B. H. Hong, K. T. Nam, *Energy Environ. Sci.* **2013**, *6*, 3658; b) N. S. Lewis, *J. Electrochem. Soc.* **1984**, *131*, 2496.

[43]   a) M. Rahman, K. Davey, S.-Z. Qiao, *Adv. Funct. Mater.* **2017**, *27*, 1606129; b) M. Z. Rahman, *Renewable Sustainable Energy Rev.* **2014**, *30*, 734.

[44]   a) S. Karlsson, J. Boixel, Y. Pellegrin, E. Blart, H.-C. Becker, F. Odobel, L. Hammarström, *J. Am. Chem. Soc.* **2010**, *132*, 17977; b) S. Karlsson, J. Boixel, Y. Pellegrin, E. Blart, H.-C. Becker, F. Odobel, L. Hammarström, *Faraday Discuss.* **2012**, *155*, 233.

[45]   T. Lopes, L. Andrade, H. A. Ribeiro, A. Mendes, *Int. J. Hydrogen Energy* **2010**, *35*, 11601.

[46]   a) D. Merki, H. Vrubel, L. Rovelli, S. Fierro, X. Hu, *Chem. Sci.* **2012**, *3*, 2515; b) J. Duan, S. Chen, M. Jaroniec, S. Z. Qiao, *ACS Nano* **2015**, *9*, 931.

[47]   Y. Zheng, Y. Jiao, L. Ge, M. Jaroniec, S. Z. Qiao, *Angew. Chem.* **2013**, *125*, 3192.

[48]   J. Zhang, J. Yu, M. Jaroniec, J. R. Gong, *Nano Lett.* **2012**, *12*, 4584.

[49]   L.-C. Chen, C.-Y. Teng, C.-Y. Lin, H.-Y. Chang, S.-J. Chen, H. Teng, *Adv. Energy Mater.* **2016**, *6*, 1600719.

[50]   J. Liu, Y. Liu, N. Liu, Y. Han, X. Zhang, H. Huang, Y. Lifshitz, S.-T. Lee, J. Zhong, Z. Kang, *Science* **2015**, *347*, 970.
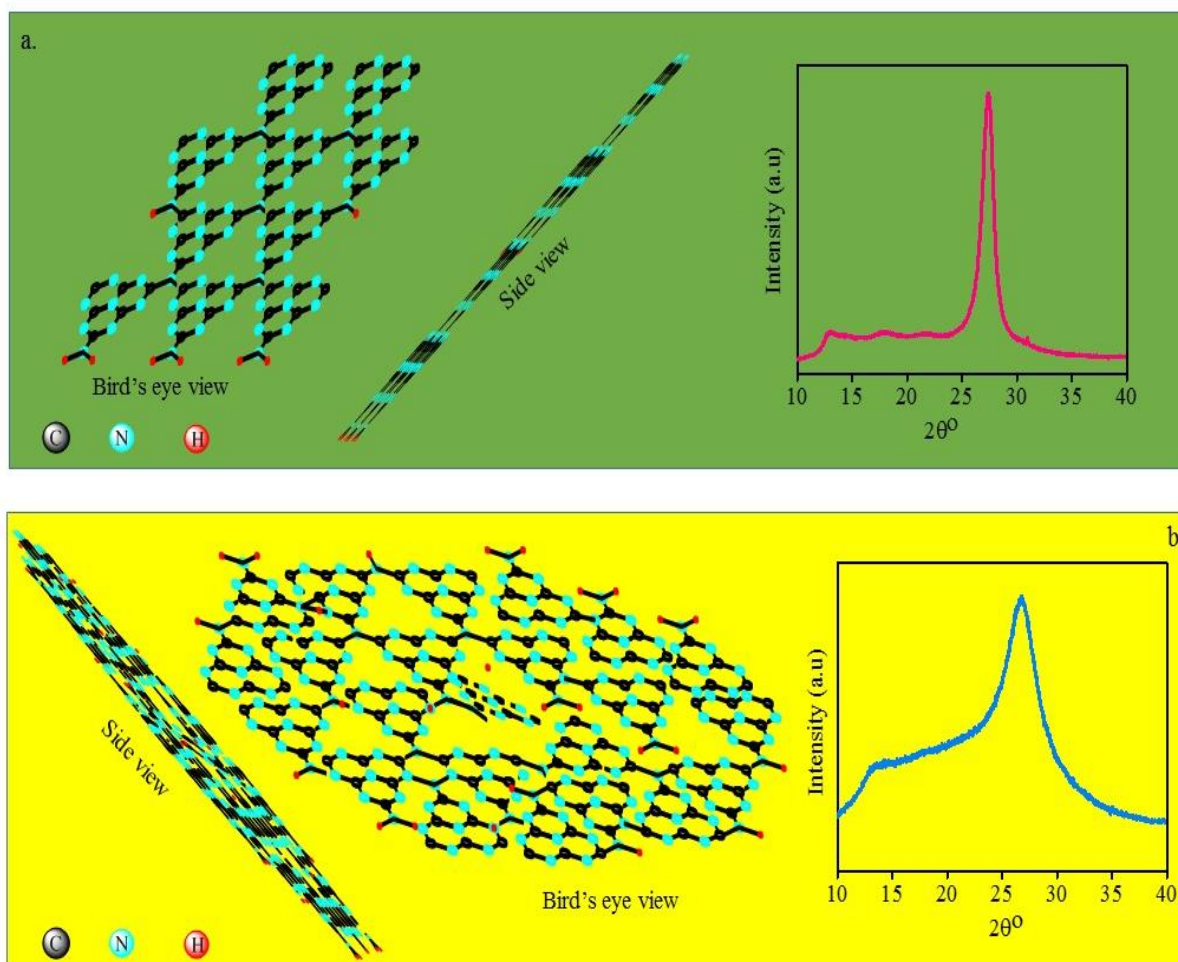
21

Figure 1. a) Atomic structure (bird's-eye view and side view) and XRD patterns of crystalline carbon nitride. A long range ordered atomic arrangement of carbon and nitrogen is discernible from different angles. The sharp peaks in XRD patterns are the result of this long range ordered atomic arrangement. b) Atomic structures (bird's-eye view and side view) and XRD patterns of amorphous carbon nitride. A long range ordered atomic arrangement of carbon and nitrogen is absence but short range atomic order is discernible from different angles. The relatively flat peaks peaks in XRD patterns are the result of the absence of long range ordered atomic arrangement.
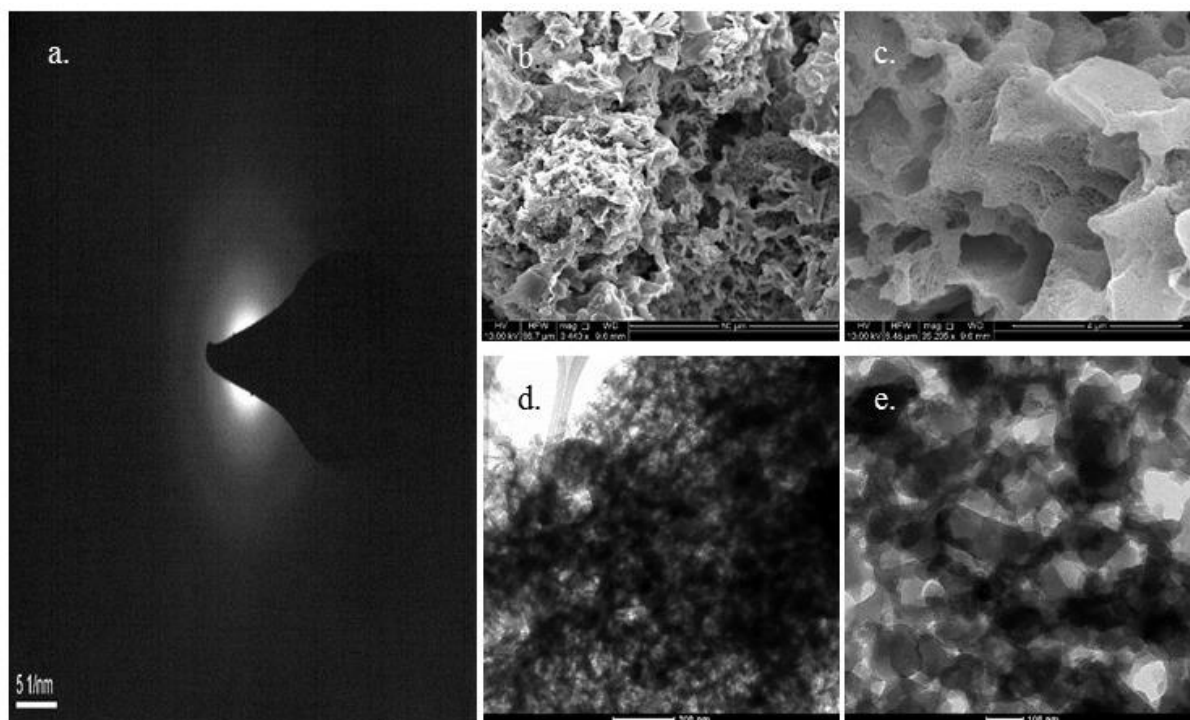
Figure 2. Morphology and structure of a-CN sponge. a) SAED pattern showing highly diffused rings, typical for amorphous materials. b) SEM image with scale-bar 50 µm representing a top view of sponge-structure with porous micro-channel. c) Enlarged SEM image with scale-bar 4 µm. This image represents a cross-sectional view of the basal planes incorporating the edges of hollow ductile. The edges are decorated with micro-mesopores. d) TEM image with scale-bar 200 nm. The voids over the image resemble the pores which are distributed over the entire surface area. e) Extended TEM image with scale-bar 100 nm - revealing the porous, spongy-structure originating from random overlapping of nanosheets.
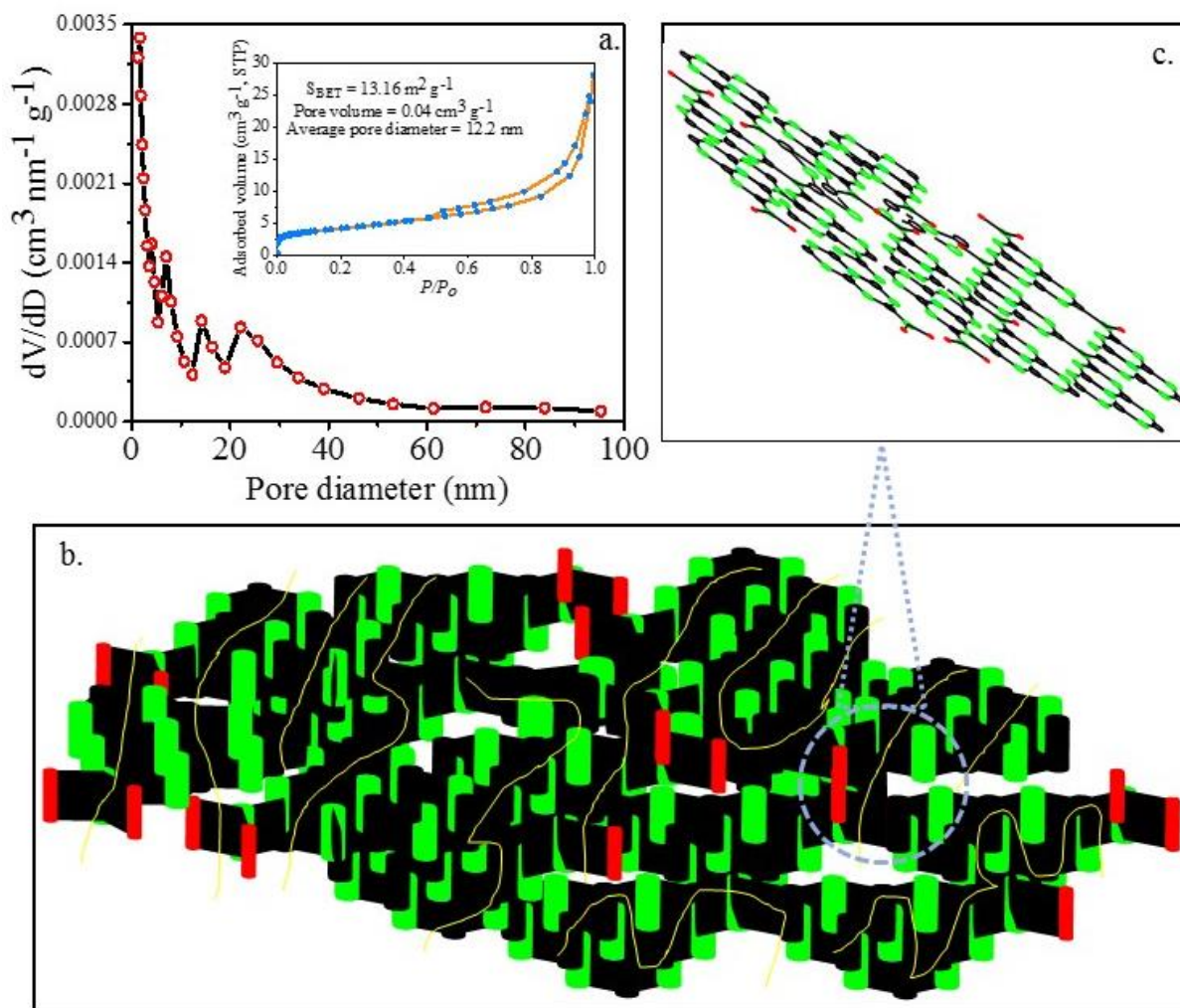
Figure 3. a) BJH pore size distribution of a-CN sponge. Inset is the result of BET surface area measurement. b) 3D perspective view at 0º of molecular structure of a-CN sponge. The trace of micro-channels is marked with gold-lines. These channels facilitate the transport of reactant molecules to reactive sites and internal reflection of incident light. c) Inside the structure at molecular level. Color codes: black for carbon, green for nitrogen and red for hydrogen.
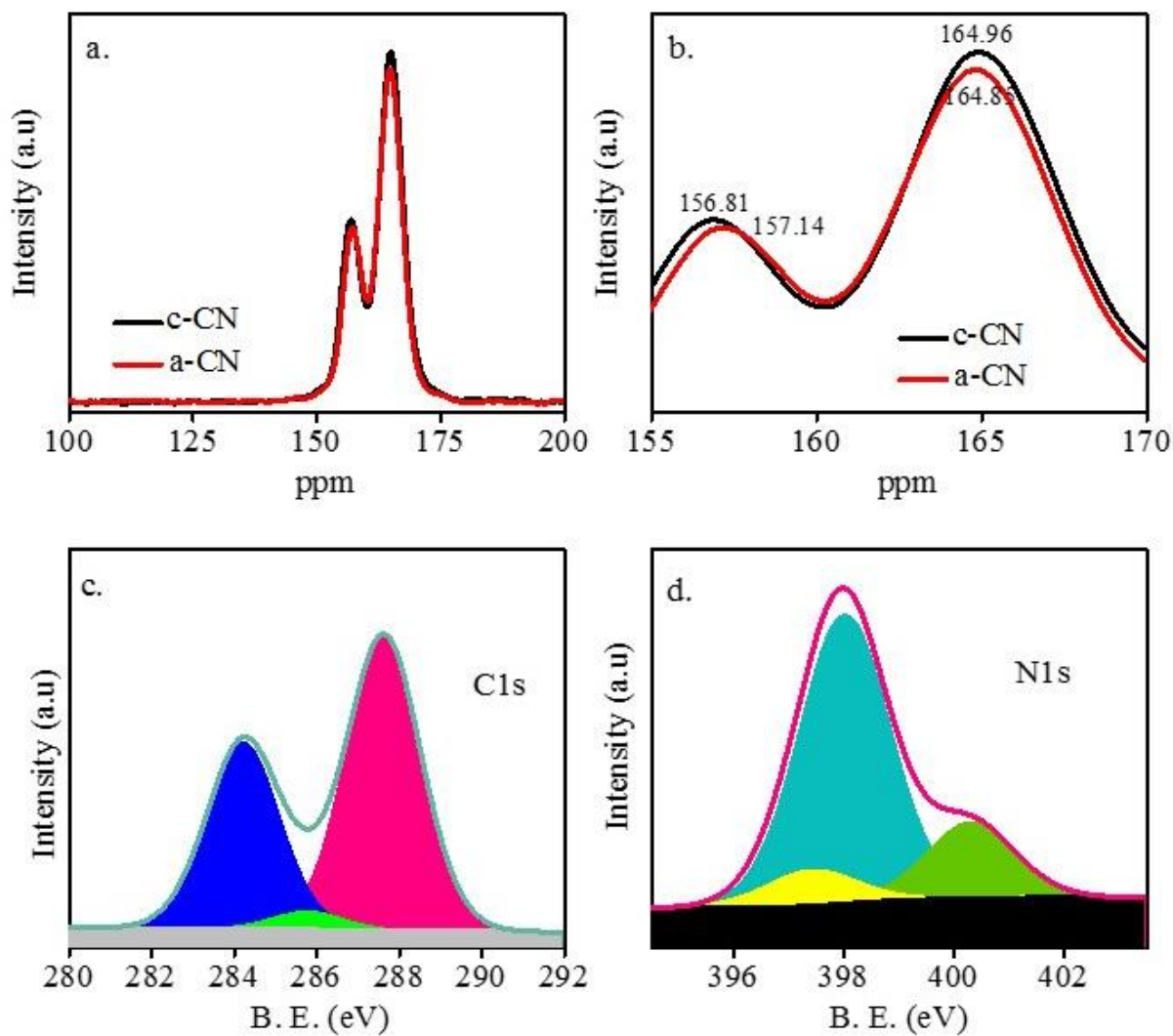
Figure 4. Chemical properties. a) Solid-state ^{13}C CP-NMR spectra of c-CN and a-CN. b) Extended ^{13}C CP-NMR spectra of c-CN and a-CN. c) Deconvoluted XPS C1s spectra of a-CN. d) Deconvoluted XPS N1s spectra of a-CN.
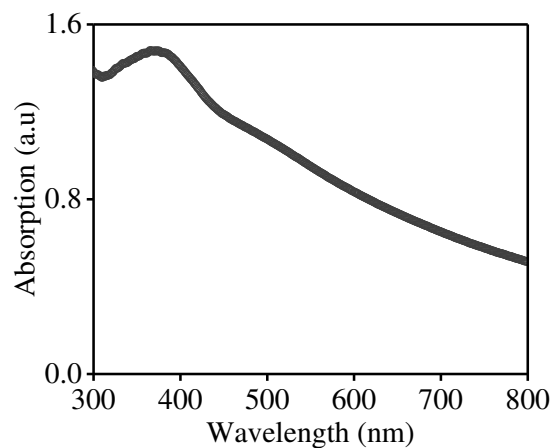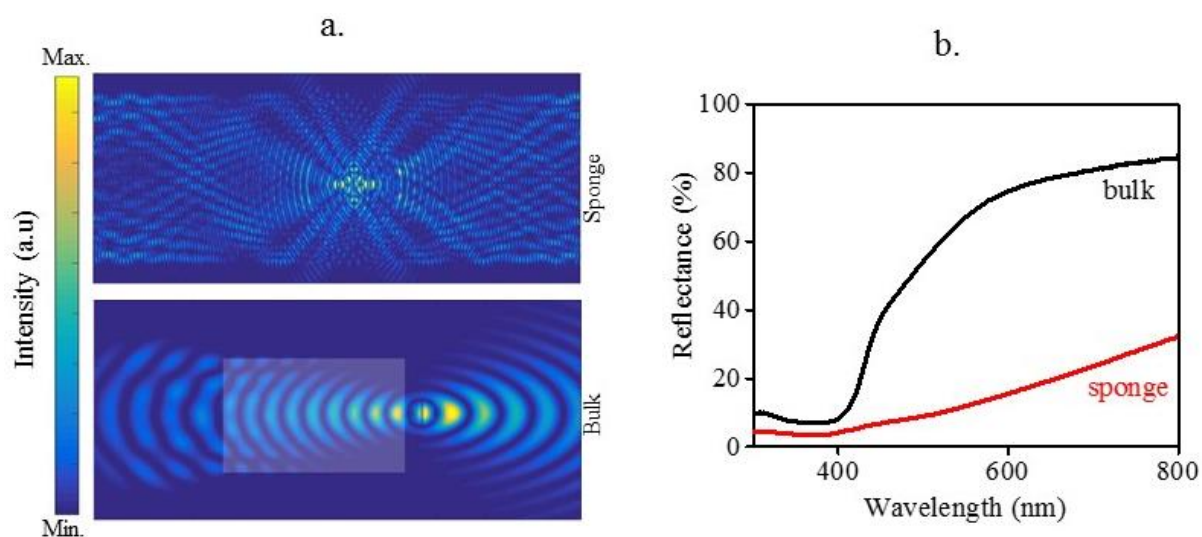
Figure 5. UV-Vis spectra of a-CN sponge.

Figure 6. a) Behaviour of light when propagating through spongy and bulk a-CN. b) Diffused reflectance spectra of spongy and bulk a-CN.
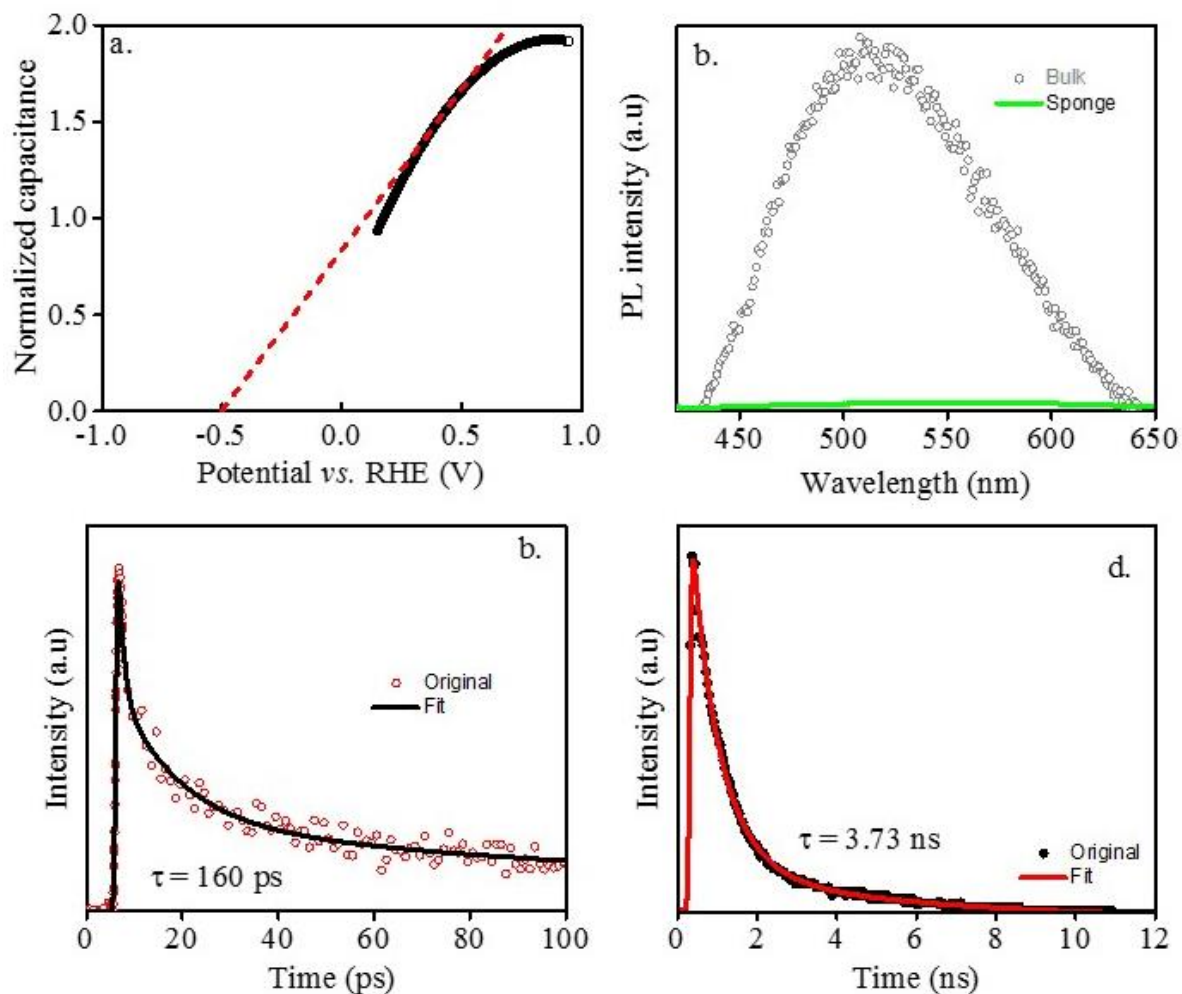
26

Figure 7. Quasi Fermi level (QFL), and charge carrier recombination and separation. a) Mott-Schottky plot for determining QFL for a-CN sponge. b) Combined PL spectra of bulk and spongy a-CN. c) Time resolved fluorescence of bulk a-CN. d) Time resolved fluorescence of spongy a-CN.
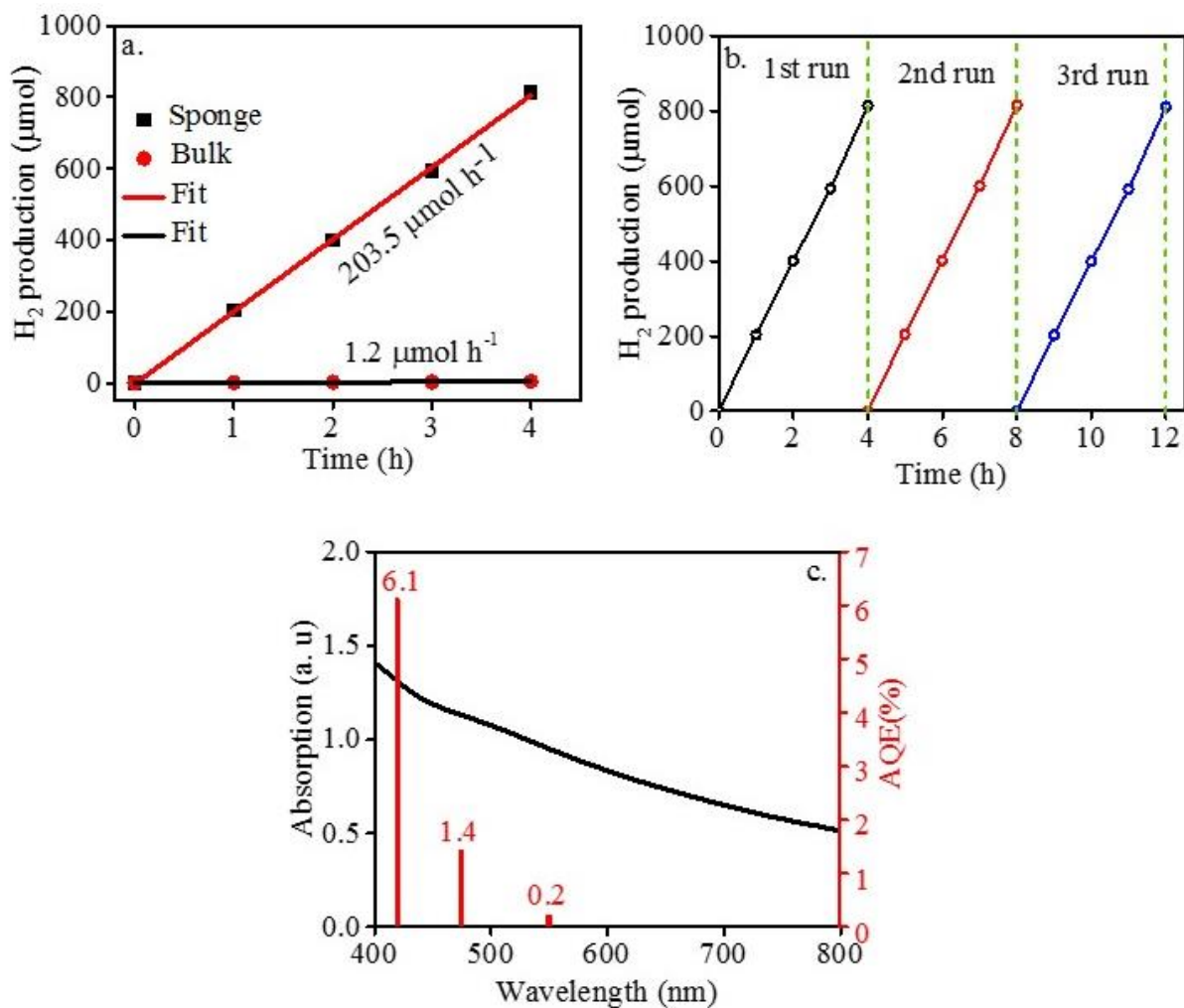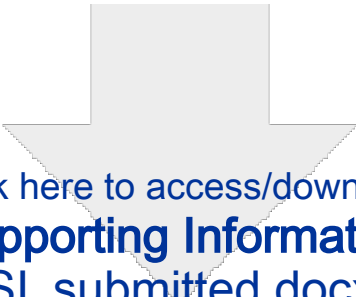
Figure 8. Photocatalytic activities. a) Average rate of hydrogen production (λ = 420 nm) by bulk and spongy a-CN. b) Cyclic hydrogen production by a-CN sponge under visible light irradiation (λ = 420 nm). Between each run, the reaction system was stored for 15 days. c) Wavelength dependent AQE by a-CN sponge.